CRYOGENIC CATHODOLUMINESCENCE FROM $Cu_xAg_{1-x}InSe_2$ THIN FILMS

Angel R. Aquino[1], Angus A. Rockett[1], Scott A. Little[2], and Sylvain Marsillac[2]
[1]Department of Materials Science and Engineering, University of Illinois, Urbana Illinois 61801 USA
[2] Wright Center for Photovoltaics Innovation and Commercialization, University of Toledo, Toledo Ohio 43606 USA

ABSTRACT

$Cu_xAg_{1-x}InSe_2$ (CAIS) thin films were deposited by a hybrid magnetron sputtering/evaporation process over a range of x values. Cryogenic cathodoluminescence (CL) data was obtained from these thin films. Emission peaks were identified and spectrally-resolved images were recorded at these wavelengths. A power-dependent CL series was also recorded. Emissions were fairly uniform across the sample for $AgInSe_2$ (AIS) (x=0). As x increased, the emission became less uniform both in intensity and in spectral components. AIS showed no significant difference between grain and grain boundary emission, while some grain boundaries in CAIS with x>0 showed higher emission intensity than the grains. No reduction in emission intensity was seen from topmost surface features in AIS, as opposed to CIS. $Cu_{0.6}Ag_{0.4}InSe_2$ showed the largest variation in emission from grain to grain, while CIS showed the largest variation in emission from grain to grain boundary.

INTRODUCTION

I-III-VI_2 chalcopyrite semiconductors are among the most studied materials for solar cell absorber layers. The bandgaps of the I-III-VI_2 system (I-Cu,Ag; III-Ga,In; VI-S,Se) cover almost the entire solar spectrum (1.07 eV – 2.73 eV), which makes it an ideal system for multijunction solar cells (see Fig. 1). However, many of these make inefficient solar cells and their properties are poorly understood, making device improvement difficult. Among these alloys, $CuIn_xGa_{1-x}Se_2$ (CIGS) has received the most attention because of its large absorption coefficient (~10^5 cm^{-1})[1] and its successful implementation in solar cells (~20% efficiency)[2,3]. The success of this alloy has led to interest in similar compounds and their properties. One such compound is $AgInSe_2$ (AIS). Its higher bandgap (1.22 eV)[4] and similarity to CIGS make it a good candidate for solar cell applications. Here we present results of the first cryogenic CL experiments with spectral imaging on $Cu_xAg_{1-x}InSe_2$ (CAIS) thin films.

The purpose of this work was to study the emission spectrum of grains and grain boundaries in CAIS in order to identify any differences among them. A decrease in emission intensity from the grain boundary would indicate a possible increase in non-radiative recombination there, which could be detrimental for solar cell devices. Spectral image acquisition allows us to see what location a specific emission is coming from, helping us to determine whether certain impurities or defects are responsible for particular parts of the emission spectrum.

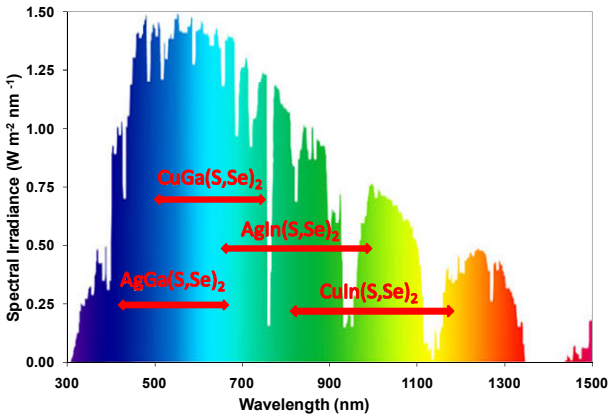

Figure 1 I-III-VI_2 system bandgaps overlaid on AM 1.5 solar spectrum.

EXPERIMENTAL

CAIS polycrystalline samples were deposited via a hybrid process in which Cu, Ag, and In were sputtered and elemental Se was evaporated. These elements were deposited onto a bare glass substrate held at 550°C. Three of these films are studied in this report.

Croygenic CL was performed on as-deposited air-exposed films. The experiments were carried out in a JEOL (JSM-7000F) scanning electron microscope (SEM) fitted with a liquid nitrogen-cooled stage and a Gatan MonoCL3 cathodoluminescence spectrometer that used a liquid nitrogen-cooled Ge photodetector. The electron beam accelerating voltage was set at 15 kV and the current at 200 pA, except where otherwise noted. Power-dependent CL spectra were also collected in order to study the behavior of the peaks. Accelerating voltages remained constant (15kV) while excitation currents were varied from 22 pA to 160 nA. The sample temperature was 5 K when the spectra were collected.

Monochromatic CL spectra were collected and analyzed. Spectrally-resolved CL images were obtained at selected positions. These spectrally resolved images were then given individual colors and overlaid in order to highlight spatial and spectral variations in luminescence. Panchromatic images (sensitive to all wavelengths of light) were also recorded for each sample.

RESULTS AND DISCUSSION

978-1-4244-5892-9/10/$26.00 ©2010 IEEE

$AgInSe_2$ sample

The surface morphology of a sample of AIS is shown in Figure 2a. The image suggests an average grain size of ~200 nm. A monochromatic CL spectrum was taken at 30kx magnification from this area and is shown in Figure 3. A best fit to the CL data was obtained for a Gaussian peak at 1020 nm (1.215 eV, FWHM = 34.7 meV) combined with an exponential tail on the lower energy side, which decayed at a rate of 44 meV/decade. Spectral images were acquired at the peak position and along the band tail (1010 nm, 1020 nm, and 1060 nm). The spectral images have been overlaid in Figure 2b. The emission at 1060 nm is colorized as red, while the 1010 nm and 1020 nm emissions contribute blue and green to the overlay, respectively. The spectral image at 1010 nm shows better lateral resolution than the 1060 nm spectral image, suggesting that the emission at 1010 nm is more localized than the emission at 1060 nm. A panchromatic CL image was also collected for this sample (see Fig. 4). Again, emissions are very uniform. Most dark areas in the panchromatic CL image correspond to dark areas in the secondary electron image (SEI).

The spectral images show no significant difference in distribution of emission with respect to position indicating compositional uniformity, unlike the samples with x>0, as discussed below. By comparing the SEI to the CL spectral image, we can see that the majority of grains exhibit some type of emission. The AIS sample is affected relatively little by protuberant surface features, meaning moderate non-radiative surface recombination. Another important observation is that grain boundaries in this sample do not appear to luminesce more or less than the surrounding grains. This means that the grain boundaries are not acting as non-radiative recombination centers.

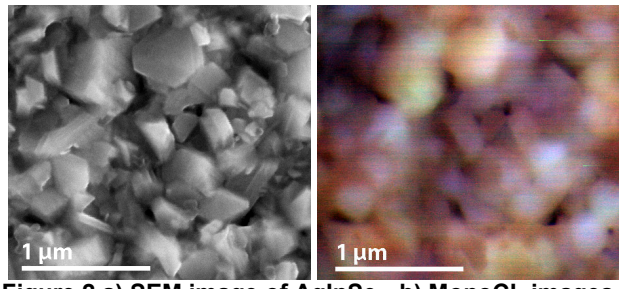

Figure 2 a) SEM image of $AgInSe_2$, b) MonoCL images overlaid with 1010 nm in the blue channel, 1020 nm in the green channel and 1060 nm in the red channel (taken in same area as Fig. 2a).

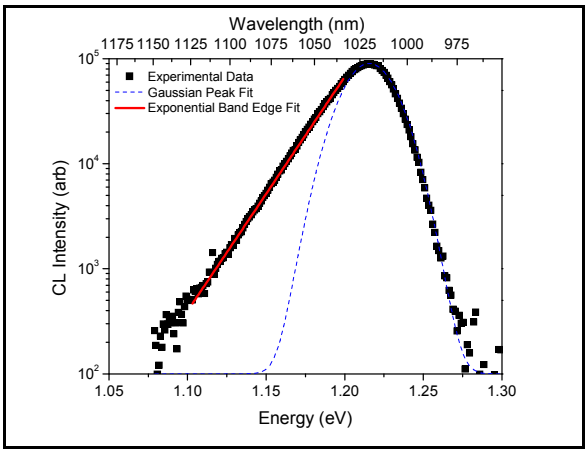

Figure 3 AIS MonoCL spectrum with best fits on area shown in Fig. 2a.

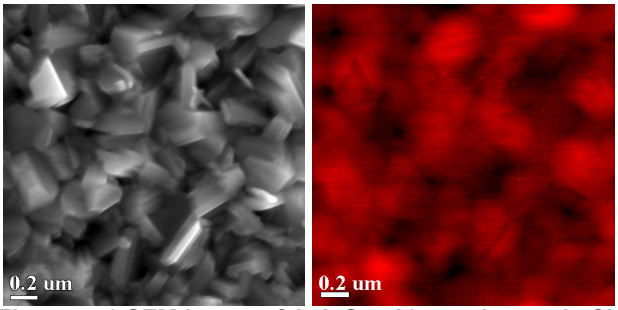

Figure 4 a) SEM image of $AgInSe_2$, b) panchromatic CL image from Fig. 4a.

Power-dependent CL spectra are plotted on a semi-logarithmic scale in Fig. 5. The spectra from 22 pA up to 640 pA can be modeled using a Gaussian peak with an exponential band tail. The Gaussian peak undergoes a blue-shift from 1028 nm (1.206 eV) to 1011 nm (1.226 eV) as power increases in this range (22 pA - 640 pA). When the excitation current is increased past 2,560 pA, second and third exponential tails are observed at the low energy (> 1168 nm) and high energy ends (< 950 nm), respectively. The Gaussian peak continues blue-shifting with increasing excitation current until reaching a maximum shift of 41 meV at 40,960 pA (994 nm, 1.247 eV). At higher excitation currents this peak experiences a red-shift.

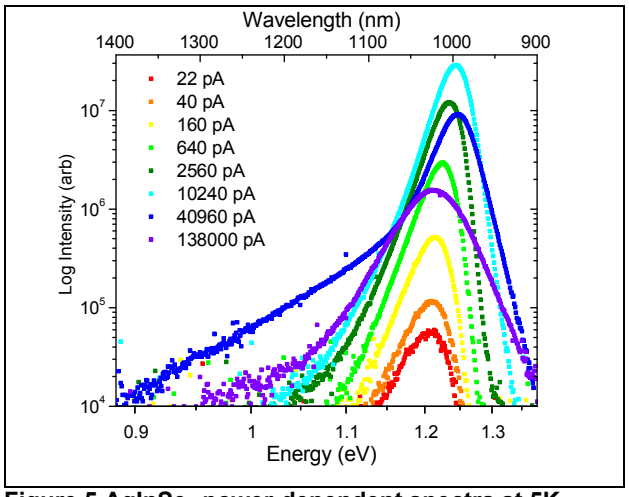

Figure 5 $AgInSe_2$ power-dependent spectra at 5K.

$Cu_{0.6}Ag_{0.4}InSe_2$ sample

A secondary electron image from the $Cu_{0.6}Ag_{0.4}InSe_2$ (CAIS) sample is shown in Figure 6. This image suggests an average grain size of ~500 nm in this sample. CL emission spectra were acquired at 1200 nm (blue channel), 1230 nm (green channel), and 1280 nm (red channel) and the overlay image is shown in Figure 6b. This sample exhibits a lot more spatial and spectral variation than the other samples. There was some enhanced emission seen from the grain boundary areas in the mono CL overlay. The white areas (see Fig. 6b) indicate the presence of all three emission wavelengths, and these seem to lie across grain boundary or inter-grain areas. This sample has the most variation of emissions from grain to grain. Some grains appear to luminesce only at one wavelength, and others do not luminesce at all. This indicates that there are compositional or electrically-active defect fluctuations between grains.

A panchromatic CL image (see Fig. 7) confirms these observations and reveals a severe reduction in emission intensity from protuberant surface features. Enhanced emission intensity from grain boundary areas is also seen. In fact, most of the red areas (more intense emission) in the image correspond to grain boundary areas in the SEM image. The dark areas in the panchromatic CL image correspond to protruding features in the SEM image.

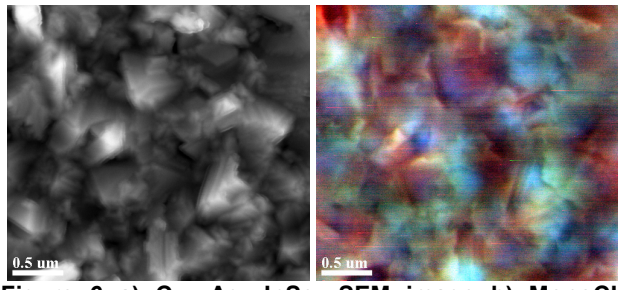

Figure 6 a) $Cu_{0.6}Ag_{0.4}InSe_2$ SEM image b) MonoCL images overlaid with 1200 nm in the blue channel, 1230 nm in the green channel and 1280 nm in the red channel (taken in same area as Fig. 6a).

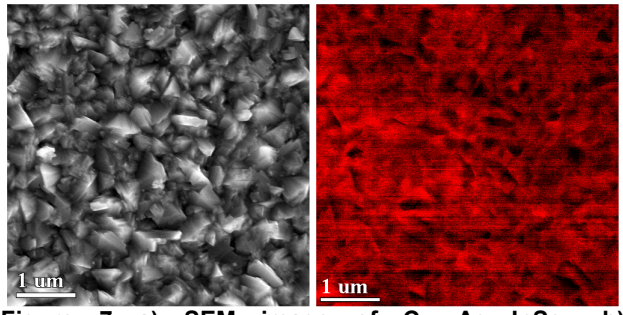

Figure 7 a) SEM image of $Cu_{0.6}Ag_{0.4}InSe_2$, b) panchromatic CL image from Fig. 7a.

Power-dependent spectra for the CAIS sample are broader than the emissions from the AIS sample. Two Gaussian peaks at 1229 nm (1.01 eV) and 1270 nm (0.976 eV) are required to obtain a best fit for the 22 and 40 pA spectra. As the excitation power is increased, exponential tails appear on both high and low energy sides of the peak, as for the AIS sample. Both Gaussian components blue-shift (20 meV and 15 meV) with increasing excitation power, but not as much as the peaks for the AIS sample (41 meV). A very broad additional Gaussian component is also present at very high excitation powers, as seen in Fig. 8 for 160000 pA.

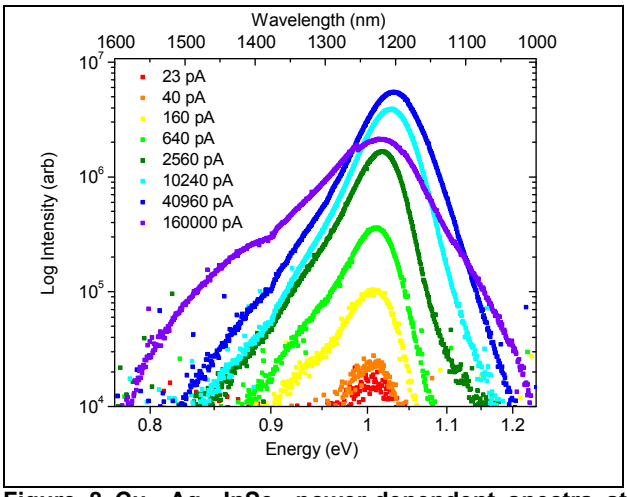

Figure 8 $Cu_{0.6}Ag_{0.4}InSe_2$ power-dependent spectra at 5K.

$CuInSe_2$ sample

A secondary electron image for the pure CIS sample is shown in Figure 9a and suggests an average grain size of ~1000 nm. Emission spectra were acquired at 1260 nm (blue channel), 1300 nm (green channel), and 1450 nm (red channel) wavelengths and the overlay image is shown in Figure 9b. This sample also exhibits a lot of spatial and spectral variation. The red emission from this spectrum was fairly uniform throughout the sample, but

with higher intensity inside the grains. This was true even close to surface facets and grain boundary edges. The other emission peaks did not luminesce well in these areas. However, the blue and green emissions were very strong near the grain boundaries. This behavior in emissions indicates that there are compositional or electrically-active defects present near or at the grain boundaries.

A panchromatic CL image (see Fig. 10) reveals a severe reduction in emission intensity from protuberant surface features and facets. Most grains appear to luminesce fairly well from the center regions. Enhanced emission intensity from grain boundary areas is also seen in the panchromatic CL image, confirming the monochromatic CL results.

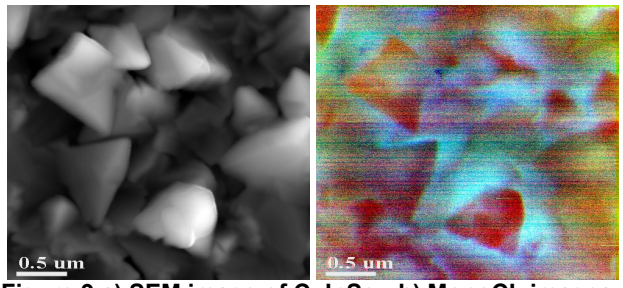

Figure 9 a) SEM image of $CuInSe_2$, b) MonoCL images overlaid with 1260 nm in the blue channel, 1300 nm in the green channel and 1450 nm in the red channel (taken in same area as Fig. 9a).

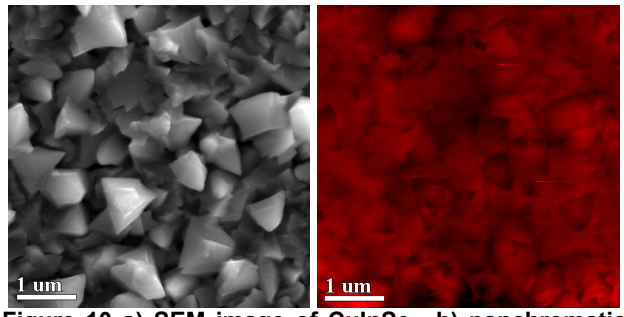

Figure 10 a) SEM image of $CuInSe_2$, b) panchromatic CL image from Fig. 10a.

The power-dependent CL series (see Fig. 11) shows even broader emissions for the CIS sample (FWHM = 95 meV for the 160 pA spectrum), even though the individual peaks required to fit the data do not get broader. In fact, 4 or more Gaussian peaks are necessary in order to obtain a best fit for the data. All peaks blue-shift 22-32 meV with increasing power and an additional peak at higher energies (1201 nm, 1.03 eV) is observed above 640 pA. These spectra also seem to have high and low energy exponential tails, especially at high powers, although more analysis will be necessary to fully understand the behavior.

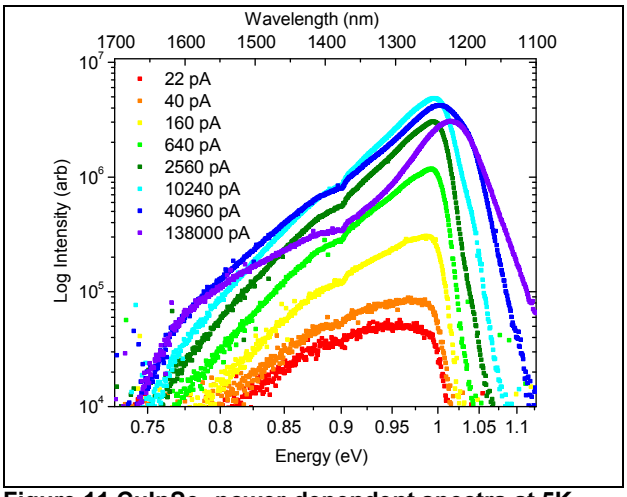

Figure 11 $CuInSe_2$ power-dependent spectra at 5K.

CONCLUSIONS

In summary, cryogenic CL experiments have been performed on CAIS thin films. Emissions from AIS are more uniform both spatially and spectrally than Cu-containing samples. AIS is also less affected by reduced emission from surface features, presumably due to less surface recombination. Cu-containing samples exhibit enhanced luminescence from grain boundaries or inter-grain areas and localized luminescent variations indicative of compositional or electrically-active defect fluctuations. This was more apparent from grain to grain in the CAIS, as it showed the most variation among the samples in emission from one grain to another. The CIS sample showed the most variation in emission from grain to grain boundary, indicating possible chemical fluctuations at the grain boundaries. As the Cu content in the films increases, emissions get broader indicating a larger number of specific defect states (more local chemical variation). Further experiments, such as temperature-dependent measurements of the Hall Effect, CL and PL will be necessary to fully characterize the transitions and assign defect levels to each. Local chemistry probes, such as transmission electron microscopy combined with energy dispersive x-ray spectroscopy, will help confirm changes in chemistry between grains and their boundaries.

The results presented here have implications for device operation. First, the relatively uniform luminescence from the AIS sample suggests that this material may produce more uniform cell performances, because reduced fluctuations in chemical composition and band structure from one location to another would result in more efficient energy collection. Variations in band structure would shunt the device locally, leading to low current high voltage grains with large energy gaps being shunted by adjacent high current low energy gap grains. The more uniform behavior in the AIS should produce better performance. At the same time, reduced surface recombination in air-exposed samples could result in less

air-sensitivity during manufacture of AIS based devices and in less dependence on a particular method for forming the current collecting heterojunction.

ACKNOWLEDGEMENT

The authors wish to acknowledge Jim Mabon for assisting with the JEOL 7000F SEM and CL setups. This work was funded by Air Force Research Laboratory contract FA9453-08-C-0172, Space Vehicles Directorate, Kirtland AFB and was carried out in part in the Center for Microanalysis of Materials at the Frederick Seitz Materials Research Laboratory at the University of Illinois, which is partially supported by the U.S. Department of Energy under grants DE-FG02-07ER46453 and DE-FG02-07ER46471. Toledo acknowledges: Ohio Department of Development (ODOD), Wright Center for Photovoltaics Innovation and Commercialization (PVIC).

REFERENCES

[1] Tuttle, J.R.; Albin, D.; Matson, R.J.; Noufi, R., *Journal of Applied Physics*, v **66**, n 9, 1 Nov. 1989, p 4408-17.

[2] Repins I, Contreras M, Romero Y, Yan Y, Metzger W, Li J, Johnston S, Egaas B, DeHart C, Scharf J, McCandless BE, Noufi R., *IEEE Photovoltaics Specialists Conference Record 2008*; **33,** 2008.

[3] http://www.zsw-bw.de/fileadmin/ZSW_files/Infoportal/Presseinformationen/docs/pi05-2010-ZSW-Worldrecord-TF-CIGS.pdf, Zentrum für Sonnenenergieund Wasserstoff-Forschung Baden-Württemberg (ZSW) Press release, 05/2010.

[4] S. Ozaki and S. Adachi, *J. Appl. Phys.* **100**, 113526 2006.